Bulletin of Engineering Geology and the Environment (2024) 83:350
https://doi.org/10.1007/s10064-024-03845-0

ORIGINAL PAPER

Response of landslide deformation to flood and impoundment of the Dahuaqiao Reservoir: characteristics and mechanisms

Chang Liu[1] · Xinli Hu[1] · Hongchao Zheng[1] · Chu Xu[1] · Shuangshuang Wu[2] · Xuan Wang[1] · Yabo Li[1]

Received: 26 September 2023 / Accepted: 8 July 2024 / Published online: 9 August 2024

Abstract

Extreme climate events and reservoir impoundment may cause the reactivation of ancient landslides. Understanding the evolutionary mechanisms and triggers of these landslides is crucial for evaluating their stability. The spatial and temporal deformation characteristics and reactivation mechanisms of two ancient landslides in the Dahuaqiao Reservoir were researched in detail using field investigations and in situ monitoring. The Yingpan (YP) and Lagu (LG) landslides are retrogressive landslides mainly in the creeping stage, characterized by low velocities. Flooding and impoundment are triggers of two accelerated deformations of landslides based on correlation analysis, respectively. Flooding caused a reservoir water level rapid drawdown, resulting in a loss of buttressing effect and a continual increase in seepage force, which, combined with sustained scouring, shearing, and erosion, reactivated the two landslides. During the impoundment, increasing buoyancy of the LG landslide mass resulted in decreased normal stress on the sliding surface and diminished resisting force. The LG landslide entered another accelerated deformation phase. In contrast, the YP landslide, which had been reinforced with stabilizing piles and slope toe presses, did not experience acceleration during the impoundment. Owing to the different permeability characteristics of the two landslides, rainfall has a greater impact on the LG landslide than the YP landslide. The results from this study will be invaluable for reservoir landslide disaster prevention.

Keywords Reservoir landslides · Dahuaqiao Reservoir · Landslide reactivation · Flood · Impoundment

Introduction

Hydroenergy represents an inexhaustible source of renewable and clean energy, and numerous hydroelectric power stations have been built around the world to make the best use of this energy. However, these engineering works can significantly change the hydrogeological conditions of bank slopes; massive reservoir landslides have subsequently formed or resurrected, resulting in serious fatalities and significant economic losses. For example, more than 4,000 landslides were discovered after the reservoir water level (RWL) of the Three Gorges Reservoir Area, one of the largest hydraulic engineering projects in the world, was filled (Yin et al. 2010; Tang et al. 2019a), including the Qianjiangping landslide in 2003 with direct damages of up to USD 7 million (Wang et al. 2004). Another tragic event was the Vajont landslide that occurred in Italy in 1963. Under the effect of reservoir storage and continuous heavy rain, 2.7×10^8 m³ of slope filled up half of the reservoir within 45 s, creating an instantaneous 250-meter high wave that inundated the nearby town and village, causing the death of nearly 2,000 people (Kilburn and Petley 2003). To present, many engineers and geologists have studied the influence of hydrological factors on landslide deformation, including RWL changes and precipitation (Yin et al. 2016; Huang et al. 2020a; Wu et al. 2022).

For RWL changes, current studies mainly focus on the initial impoundment and subsequent RWL fluctuations, the latter including drawdown and filling periods (Tang et al. 2019b; Yang et al. 2023). Reservoir initial impoundment implies extensive submerging of the sliding mass and sliding zone, causing a decrease in the shear strength of the landslide involved materials and a significant increase in buoyancy force, which adversely affects the landslide

✉ Xinli Hu
huxinli@cug.edu.cn

[1] Faculty of Engineering, China University of Geosciences, Wuhan 430074, China

[2] School of Geosciences and Engineering, Hohai University, Nanjing 211100, China

stability (Iqbal et al. 2018; Yi et al. 2022). Huang et al. (2016) investigated the major influencing factors of the Jinlongshan landslide at the Ertan Reservoir based on monitoring data over 25 years, covering the period before, during, and after the reservoir impoundment, which exhibited a slow creep phase before impoundment, a sharp increase in velocity during impoundment, and another slow creep phase after impoundment. However, when the permeability coefficient of the sliding mass is very small, the seepage force pointing to the slope increases landslide resistance, which instead promotes landslide stability in the early stage of impoundment (Paronuzzi et al. 2013). During the drawdown, when the RWL declines faster than the groundwater level, the dissipation of pore water pressure in the slope lags behind the reduction of external hydrostatic pressure, which generates a seepage force along the slip direction under the transient seepage and accelerates the landslide deformation (Yin et al. 2016). The cumulative displacement curve of this type of landslide, called seepage-driven landslide, usually shows an obvious step-like shape (Zhou et al. 2022). Wu et al. (2021, 2022) reported a long-monitored giant landslide located in the Jinping Reservoir and classified its deformation process into four phases: slow movement pre-impoundment; reactivated motion in the initial impoundment; significantly accelerated movement during reservoir drawdown with a rate above 500–600 mm/year; and deformation speed decreased under the following RWL fluctuations. Reservoir filling leads to softening of slope material and an increase in buoyancy force. Although these impacts are smaller than the initial impoundment, they can still aggravate deformation in some landslides (Zhao et al. 2013; Huang et al. 2020b). These landslides are often referred to as buoyancy-driven landslides, characterized by high permeability (soil-rock ratios ≤ 1), a chair-shaped sliding surface, and a linear curve of cumulative displacement (Zhou et al. 2022). At present, there are fewer reports on the effect of impoundment on the deformation characteristics of reservoir landslides reinforced with stabilizing piles.

Rainfall was found to be another important causative factor for reservoir landslides (Huang et al. 2020a; Shi et al. 2021). Continuous or heavy rainfall raises the water table after infiltrating the landslide (Wang et al. 2022), increasing the pore water pressure, and reducing the effective stress, while adding the weight of the sliding mass, weakening the shear strength of the sliding zone, and causing slope destabilization (Collins and Znidarcic 2004; Rahardjo et al. 2007; Ran et al. 2018). Normally, the rainy season is followed by a drop in RWL; hence the accelerated deformation of reservoir landslides is caused by the combined effect of both (Tang et al. 2019a; Yao et al. 2019). However, long-term sustained rainfall or heavy rainfall may create flooding. There are few studies on landslide reactivation due to erosion, high-speed scouring, and rapid RWL changes caused by flooding.

The topography of southwest China has allowed for the construction and planning of a number of hydropower projects, including the Dahuaqiao hydropower station. In this study, a comprehensive analysis of deformation characteristics associated with the Yingpan (YP) landslide and the Lagu (LG) landslide located in the Dahuaqiao Reservoir was conducted based on field monitoring. Notably, the YP landslide was reinforced with stabilizing piles and slope toe pressed. To examine the causes of landslide accelerated deformation, correlation coefficients were utilized to identify the response of landslide movement to flooding, reservoir impoundment, and rainfall. In addition, the reactivation mechanisms of the two landslides were compared and some interesting conclusions were drawn. Given that further construction of hydroelectric power worldwide and extreme climate may lead to more landslides, this study provides insights into preventing and mitigating similar landslides.

Study area

The Dahuaqiao hydropower station is located in Lanping County, Yunnan Province (Fig. 1). This is the seventh dam constructed on the upper reaches of the Lancang River, with the Huangdeng and Miaowei dams situated upstream and downstream, respectively. The dam site is approximately 588 km from Kunming City and 77 km from Lanping County.

The dam is a concrete gravity dam with a crest length of 231.5 m, a dam height of 106 m, a total reservoir capacity of 2.93×10^8 m^3, and an installed capacity of 920 MW. The normal water level rests at an elevation of 1477 m, while the dead water level is at an altitude of 1472 m. The drainage area of the Dahuaqiao Reservoir is 9.26×10^4 km^2. Several areas of the front edge of the mountains have been submerged by the reservoir following its impoundment, thereby contributing to the possibility of landslides.

Geological conditions

The hydropower station is located in the middle section of the Hengduan Mountains, western Yunnan. The terrain is generally higher in the north and lower in the south, with the mountain ranges roughly oriented in a north-northwest or nearly north-south direction. Most river valleys in the reservoir area are V-shaped, showing a high and medium mountain canyon landscape.

The reservoir area lies on the southeastern edge of the Tibetan Plateau, in the southeastern arc of the

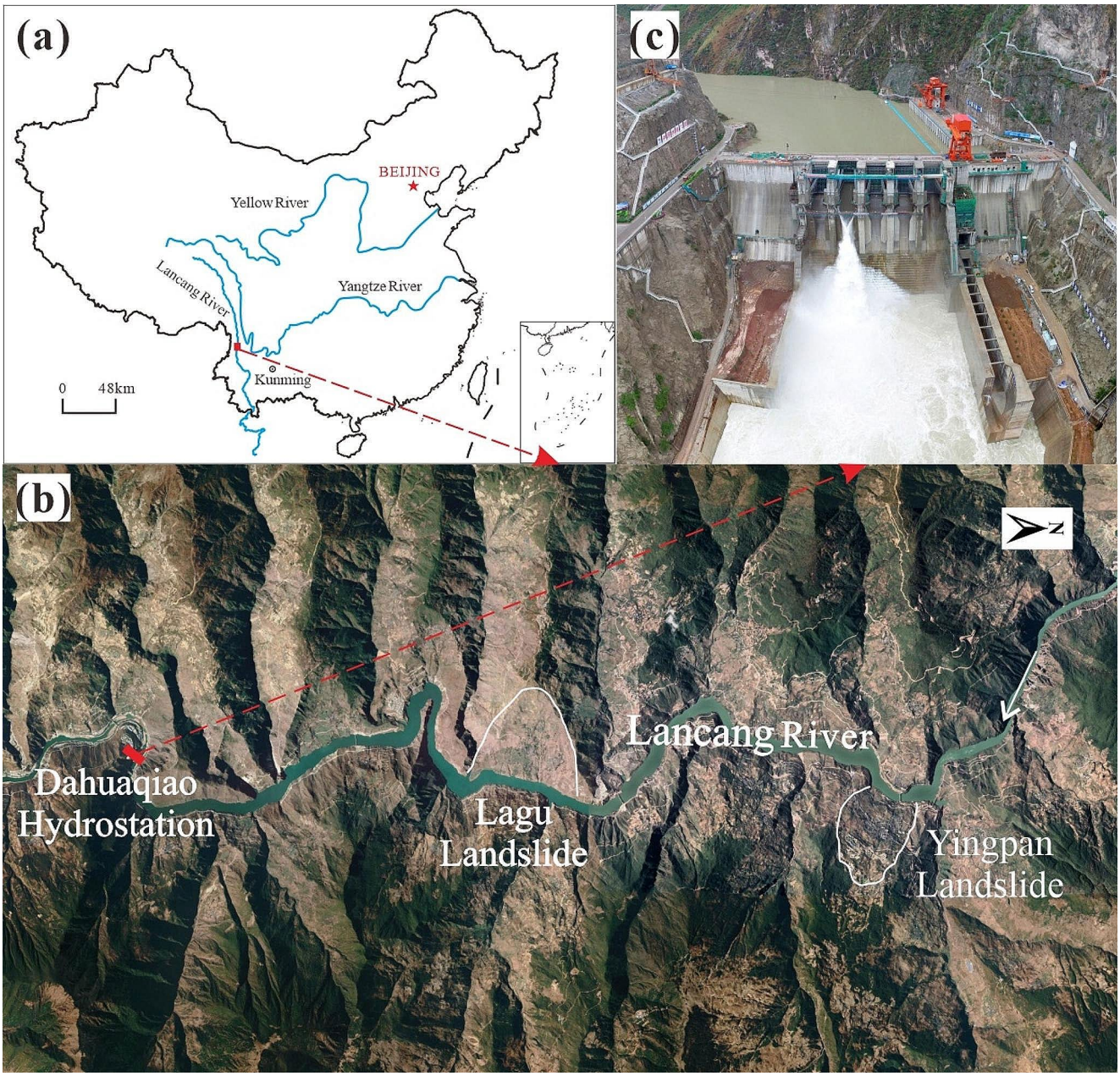

Fig. 1 Location of the study area: **a** location of the Dahuaqiao Reservoir, southwestern China; **b** location of two landslides and the dam site; **c** field overview of the Dahuaqiao hydropower station

Tethys-Himalayan tectonic domain, and is the combined part of the Yunnan-Tibetan Plate and the Yangzi Plate. The geological structure of the region is complex and has seen many periods of tectonic movement, with the most significant tectonic traces dating back to the Himalayan period. Due to the strong tectonic action, the rocks are mostly folded, faulted, and metamorphosed, and therefore easily alterable and breakable(Sun 2015; Lin et al. 2017).

Hydrological and meteorological conditions

The climate in the area is characterized by high temperatures and precipitation due to a subtropical monsoon climate. Statistically, Lanping Meteorological Station (No. 56645) indicates that the multi-year average temperature is 11.3 °C, and the average precipitation is 973.5 mm. The distribution of precipitation throughout the year is uneven: more than 71.6% of the annual precipitation falls from June to September. In contrast, from November to March, precipitation

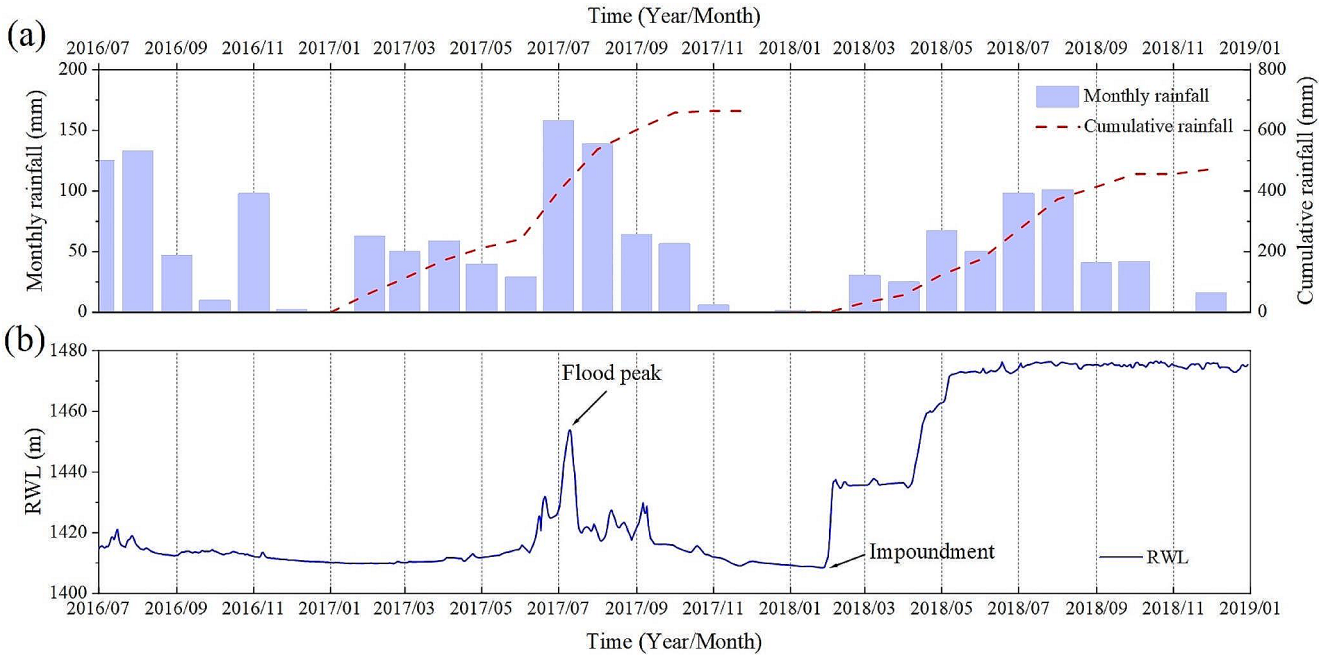

Fig. 2 Time-series of **a** rainfall and **b** RWL

Fig. 3 Field photos **a** before and **b** after flooding

is relatively low, comprising only 10.8% of the annual total (Fig. 2a).

The flood season is mainly concentrated between June and September, and major floods are mainly caused by continuous or heavy rainfall. It was observed in July 2017 that the RWL exhibited a rapid rise and fall due to heavy rainfall upstream and a restriction on the flood discharge from the diversion hole of the uncompleted hydropower station. The water level reached its highest on July 10 (Fig. 2b), with the peak flow at the dam site reaching 6120 m^3/s at 16:00, close to the 20-year return period standard, a new local record for nearly 30 years (https://www.sohu.com/a/158156455_735428), causing road disruptions and house damage, as well as reactivating some ancient landslides (Fig. 3).

In February 2018, Dahuaqiao hydropower station started impounding, and RWL started rising from 1410.97 m. As shown in Fig. 2b, the impounding process consists of two stages: Firstly, the RWL rose rapidly to 1435 m within 5 days. After waiting 80 days, the RWL gradually increased from 1435 m to 1476.5 m and then fluctuated between 1472 and 1477 m.

Landslide characteristics

There are several ancient landslides and collapsed deposits in the middle and lower reaches of the Dahuaqiao Reservoir area. To ensure the safety of the reservoir area after impoundment, several landslides were monitored before impoundment. The YP and LG landslides (Fig. 1b), which have undergone extensive monitoring, demonstrated significant responses to flooding and impoundment. Therefore, these two landslides were selected for more detailed investigation in this study.

Yingpan landslide

The YP landslide is located on the left bank of the Lancang River, 24 km from the dam (Fig. 1b), and is divided into three zones (Fig. 4a). The I# zone is in the shape of a circular chair with a length of about 900 m and a width of 1200 m, a gradient of 10 ~ 25° and a volume of about 7.0×10^6 m^3, the mean thickness of the sliding mass is about 42.5 m. The elevation of II# zone is 1590 ~ 1850 m, with a volume of about 1.0×10^7 m^3, on which is Yingpan Town. The III# zone is located at the back edge of Yingpan Town, with an elevation of 1850 ~ 2100 m and a volume of about 9.6×10^6 m^3.

The composition of the sliding mass is mainly Quaternary system (Q_4^{del}) gravel clay and silt with a small number of boulders, fractured slate, and rock debris. The permeability coefficient of the sliding mass is estimated at 1.5×10^{-6} ~ 4.3×10^{-7} m/s based on the permeability tests (Lin et al. 2017). The sliding zone mostly consists of clay, silt clay, containing gravel, with 10 ~ 25% gravel content, characterized by fine particles and poor permeability, and can be regarded as an aquiclude. According to the borehole data, the distribution of the sliding zone is discontinuous and has a thickness of 0.1 ~ 1.3 m (Lin et al. 2017). The underlying bedrock is the purple slate of the Middle Jurassic Huakaizuo Formation (J_2h) and the purple-red slate of the Upper Jurassic Bazhulu Formation (J_3b), with an average dip direction of 320° and a dip angle of 75° (Fig. 4b). The upper part of the bedrock is highly weathered or completely weathered, which is mostly dumped and broken, and the RQD (Rock Quality Designation) is very poor. The YP landslide can be defined as a retrogressive, slow, moist earth slide according to Cruden and Varnes (1996).

Yingpan Town is in the middle of the landslide, including the government, schools, hospitals, banks, etc., and a total of more than 2000 people. After reservoir impoundment, the RWL will rise about 32 m and the leading edge of the landslide will be partially submerged, deteriorating its stability. Once I# zone is broken, it will cause a large deformation in the II# zone due to the traction effect. Several treatments were taken before impoundment to avoid the development of this situation, such as stabilizing piles and slope toe pressed (Fig. 5). Stabilizing piles are employed with a circular cross-section, with a diameter of 2 m, and pile spacing of 4 ~ 6 m, totaling 222 piles. The volume of slope toe pressed is estimated to be approximately 1.38 million m^3.

Lagu landslide

The LG landslide is 12.5 km from the dam, and its elevation ranges from 1430 m to 2000 m (Fig. 6). Within the slope area, the terrain is higher in the west (rear) and lower in the east (front), and higher in the south (downstream) and lower in the north (upstream). The volume of the landslide deposit is estimated to be approximately 5.8×10^7 m^3, mean thickness is about 40 m. When the RWL reaches normal water level, the leading edge of the landslide is approximately 47 m below the water level. The LG landslide can be divided into three zones: I# zone has large deformation and long tongue shape, II# zone and III# zone are stable at present.

The sliding mass is a Quaternary soil-rock mixture consisting of crushed stone and clay, including the strongly weathered broken slate. The soil-rock mixture has a high content of crushed blocks, which are sub-angular in shape, and the crushed blocks are generally 2 ~ 15 cm in diameter and 15 ~ 30 m thick. The permeability coefficient of the sliding mass is estimated at 6.63×10^{-5} m/s based on the permeability tests of nearby landslides (Jiang et al. 2021). The sliding zone, which is found in LG-SAA1-1, LG-IN2-2, and LGIN3-1, is mostly composed of clay, mud and gray-green gravel with a grain size of 3 ~ 8 mm, sub-angular shape and content of about 30%. The bedrock is characterized by the weakly weathered purple-red slate of the Bazhulu formation of the Upper Jurassic system (J_3b) with a small amount of sandstone, with an average dip direction of 345° and a dip angle of 70°, tilting inward to the slope (Fig. 6b). The LG landslide can be defined as a retrogressive, very slow, moist earth slide according to Cruden and Varnes (1996).

Method

In order to understand the deformation characteristics of two landslides during the flood season and impoundment period, various monitoring devices were installed on the landslide (Fig. 7). The long-term monitoring system includes hydrological monitoring and measurements of surface displacement and deep displacement. The hydrological monitoring measured rainfall and RWL. A total of 21 and 17 automatic GNSS monitoring stations were used since September 2016 to measure the ground displacement of the YP and LG landslide, respectively. In addition, borehole inclinometers and SAA were used to measure the underground displacement. There were 12 borehole inclinometers and 3 sets of SAA for the YP landslide, and 11 borehole inclinometers and 2 sets of SAA for the LG landslide. These manual monitoring instruments were buried at a depth of 40 ~ 93.5 m, which exceeds the depth of the potential sliding surface. The vertical spacing of each borehole monitoring point was 0.5 m, and the frequency of data collection was 2 ~ 4 times per month.

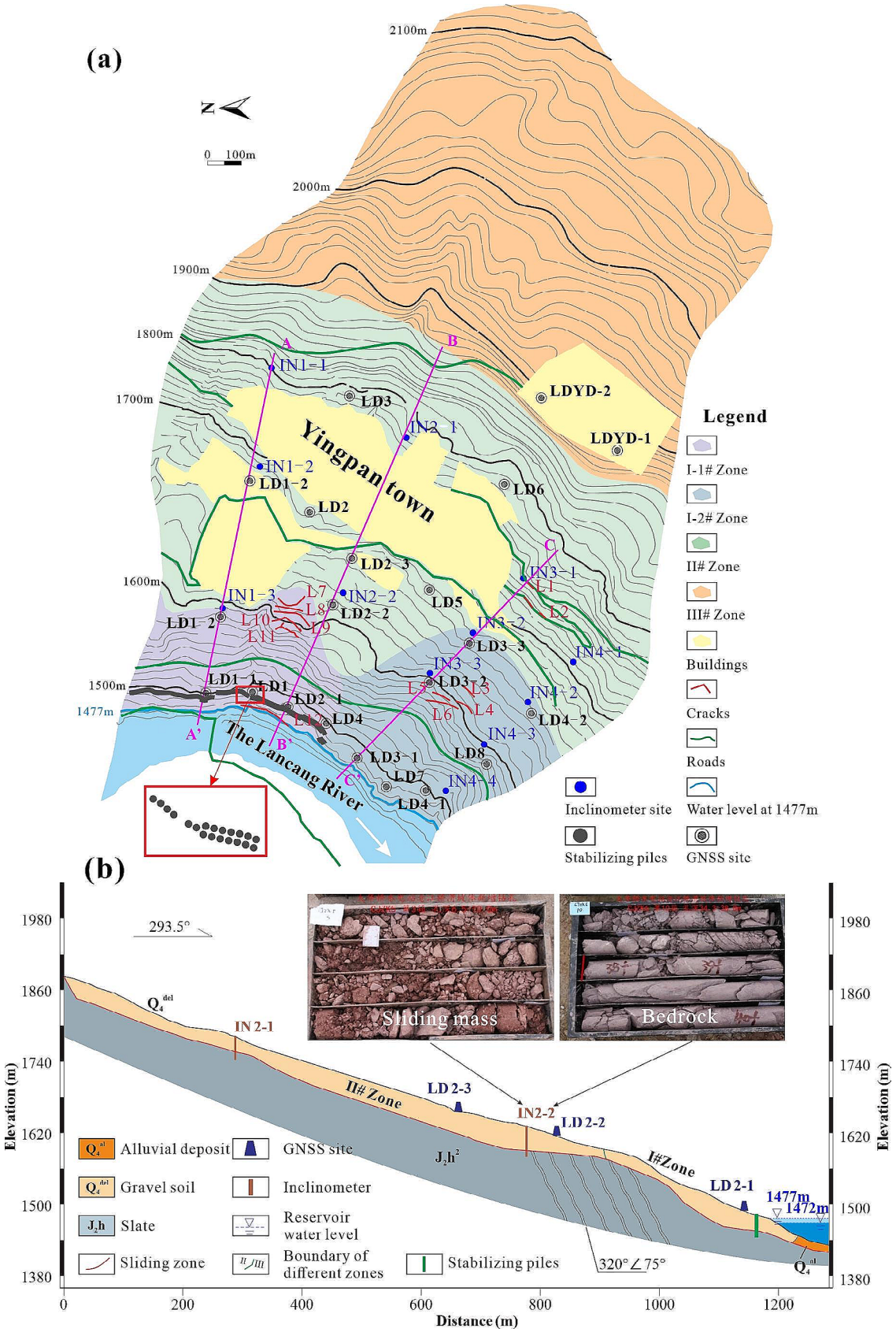

Fig. 4 YP landslide: **a** topographic map and **b** geological section map (B-B')

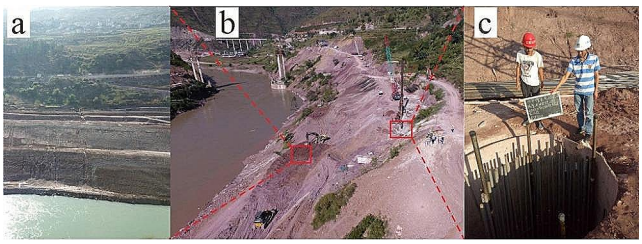

Fig. 5 Landslide control methods: a slope toe pressed, b construction, and c stabilizing piles

Results

Surface deformation

YP landslide

There were many cracks on the surface of the I-1# zone found during site investigations (Fig. 8), and the retaining wall of the road leading to Cangjiang Bridge has been deformed (Fig. 8b). The orientations of cracks L7 ~ L11 are 185 ~ 195°, perpendicular to the main slip direction. The opening of crack L7 at 1612 m a.s.l. varies by 0.5 m, and the maximum vertical dislocation is approximately 61 m (Fig. 8d). The maximum width of crack L9 is 1.7 m, and the length is 85 m (Fig. 8f). According to residents, the deformation of these cracks is mainly concentrated in the flood season, especially in 2017. Following the geological survey, no significant large deformations were discovered in the II# and III# zones, only localized shallow deformation, indicating that these areas are in a stable state. The movement of the YP landslide was from front to back.

The surface movement characteristics of the YP landslide were established based on the data from GNSS (Fig. 9). The deformation of the YP landslide was in a stage of creep characterized by retrogressive movement most of the time, which means displacements of the slope toe are significantly larger than those of the upper slope (Zhang et al. 2024). However, the landslide underwent accelerated deformation in July 2017, corresponding to the flood event.

The cumulative displacements recorded at the GNSS monitoring points YP-LD1, YP-LD4, and YP-LD2-1 reached 2472.16 mm, 2155.02 mm, and 2563.56 mm, respectively, during the monitoring period (Fig. 9a; Table 1). In contrast, the maximum displacement recorded in Zone II# was only 195.05 mm, and in Zone III#, YP-LD-YD1 and YP-LD-YD2 recorded maximum values of 11.48 mm and 25.42 mm, respectively. These results indicate that the deformation of the YP landslide was predominantly concentrated in Zone I#, particularly in the upstream I-1# zone. This is consistent with the results from field investigations, which revealed many large cracks perpendicular to the main slide direction on the downstream side of the I-1# zone (Fig. 4a). Furthermore, the statistical data in Table 1 highlight that significant deformation of the YP landslide occurred mainly in July 2017. During this month, the front monitoring points YP-LD1 and YP-LD4 registered displacements of 1403.85 mm and 1258.07 mm, respectively, whereas the middle monitoring points YP-LD2-2 and YP-LD2-3 recorded only 8.23 mm and 3.36 mm, respectively.

Figure 9b illustrates the variation in the GNSS displacement rate and the water level change rate over time. The surface displacement rate of the YP landslide was maintained between −5 ~ 10 mm/d and was in the slow creep stage most of the time. The RWL kept rising due to the strong rainfall upstream and restriction of the flood discharge from the diversion hole of Dahuaqiao hydropower station since the flood season in 2017. Then, the YP landslide deformation rate began to increase. The maximum displacement rate reached 126 mm/d, which was 10 times the slow creep rate, and the landslide entered the accelerated deformation stage (bounded by a first red box in Fig. 9b). Subsequently, after another rapid change of RWL occurred in September 2017, the landslide displacement rate increased significantly again, reaching a maximum of 61 mm/d (labeled by the second red box in Fig. 9b). However, at medium and high altitudes, the velocity of the monitoring point remained at a low level; for example, YP-LD5 was 0.07 ~ 0.14 mm/d. These results suggest that the YP landslide is a retrogressive landslide and the rapid change in RWL resulted in accelerated deformation.

Following the reservoir impoundment in February 2018, a detailed analysis of the landslide behavior showed that there was no significant acceleration in deformation. However, a slight acceleration was observed at monitoring points YP-LD7 and YP-LD3-1, located on the downstream side (Fig. 9a, labeled by the red box, and 9b, labeled by the third red box). This behavior can be ascribed to the stabilizing piles and slope toe pressed used to reinforce the I-1# zone on the upstream side before impoundment, whereas only slope toe pressed was applied in the I-2# zone. Despite the observed response of the downstream side of the landslide to the water storage process more or less, the maximum displacement rate was only 0.29 mm/day, which can still be classified as "very slow" (Hungr et al. 2014). This finding indicates that stabilizing piles are an effective method for enhancing reservoir landslide stability during impoundment, and the YP landslide re-entered in a slow creep phase.

LG landslide

There were different volumes of toe erosion-collapse appeared in the LG landslide along the river bank, especially in I# zone and II-1# zone (Fig. 10) based on field investigation. The opening degree and scope of the original local cracks in the lower part of the landslide widened with

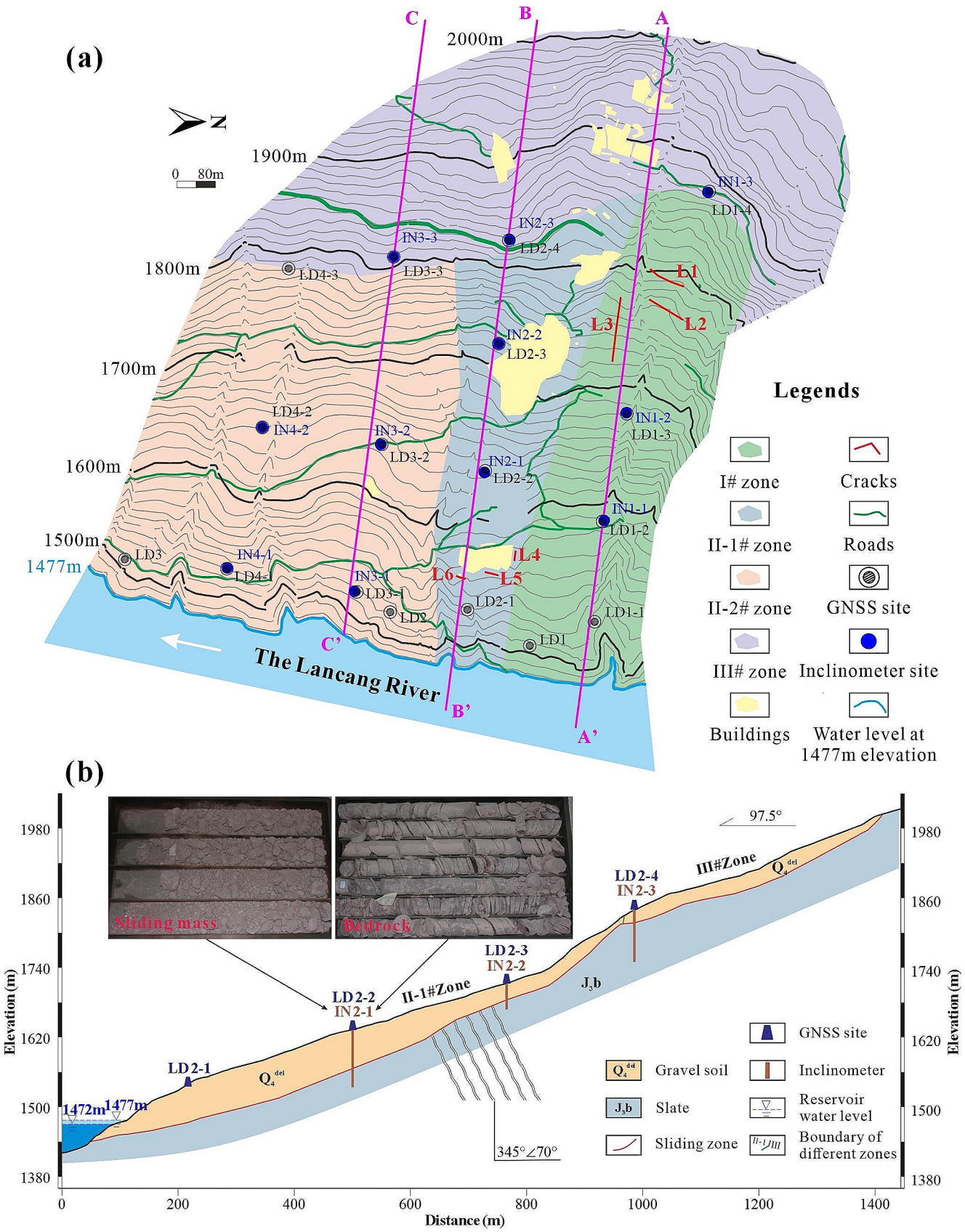

Fig. 6 LG landslide: **a** topographic map and **b** geological section map (B-B')

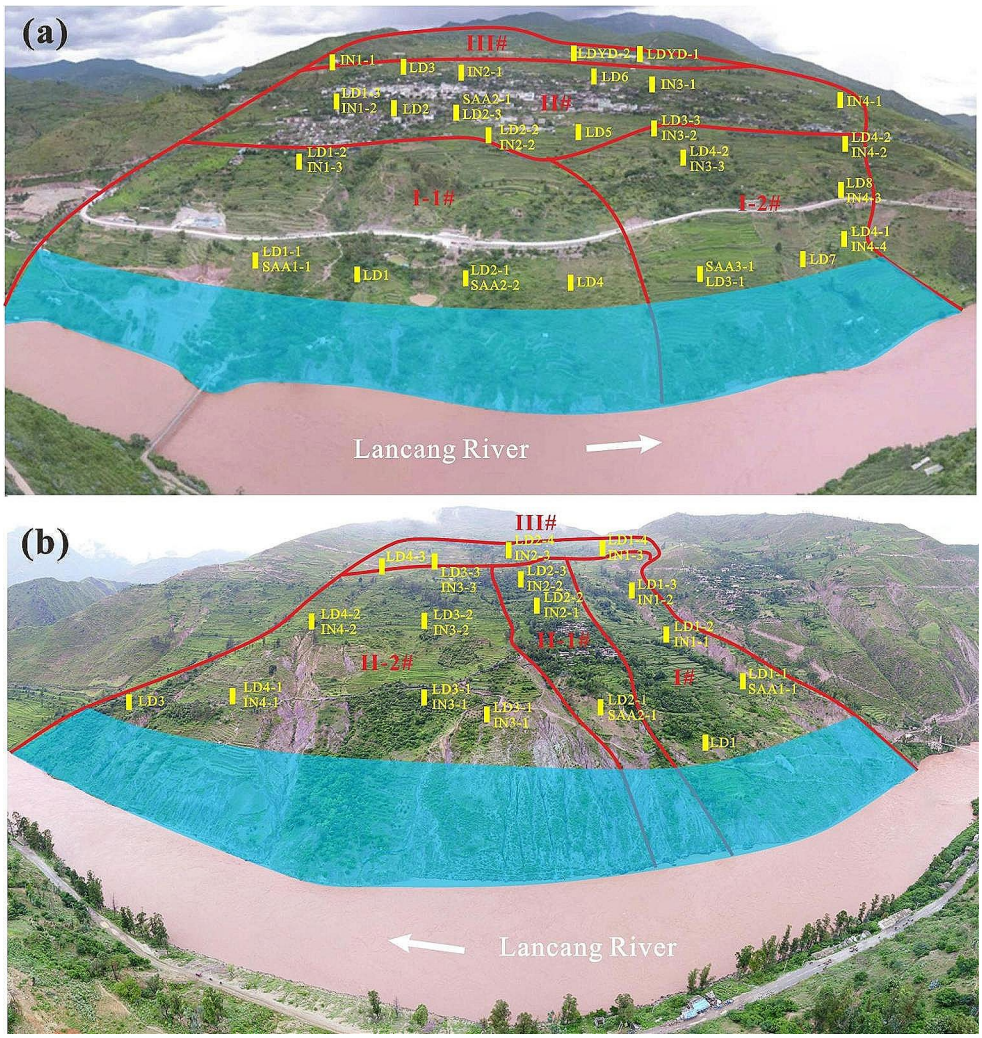

Fig. 7 Aerial photo and monitoring sites (the blue zone represents the submerged part of the landslide after impoundment): **a** YP and **b** LG landslide

the approaching flood season and the filling of the reservoir. The orientation of cracks L4 ~ L6 is perpendicular to the main slip direction. There were no obvious signs of deformation in the center and rear of the landslide.

Unlike the YP landslide, the LG landslide has exhibited two instances of rapid deformation since 2017 (Fig. 11a). The displacement is predominantly greater at the leading edge than at the back edge and more significant on the upstream side compared to the downstream side. The deformation is primarily concentrated in the I# zone. The cumulative displacements recorded at monitoring points LG-LD1, LG-LD1-1, LG-LD1-2, LG-LD1-3, LG-LD2-3, and LG-LD3-3 were 4569.02 mm, 2866.64 mm, 2012.58 mm, 821.32 mm, 70.16 mm, and 52.64 mm, respectively (Table 1).

The first accelerated deformation occurred during the flood season in 2017, corresponding to the main flood event. Figure 11b shows that the closer it is to the leading edge, the faster the landslide deformation responds to the RWL change and the greater the maximum horizontal displacement rate. Taking the monitoring profile of I# zone as an example, most blue points representing LG-LD1-1 are located above the green points representing LG-LD1-2, and the vivid amber points representing LG-LD1-3 are near the zero axis. In the LG landslide, accelerated deformation began when the RWL rose and reached its peak when it dropped rapidly (labeled by the second red box), as shown by a linear increase in displacement rate (Fig. 11b). In contrast, the YP landslide experienced accelerated deformation only at the rapid fall of the RWL, which was expressed as a sudden change in displacement rate (Fig. 9b). Another interesting phenomenon is that the LG landslide reached its maximum displacement rate and maximum monthly displacement in September, later than the YP landslide. It is plausible to hypothesize that the prolonged rainfall from June to September facilitated continued rainwater infiltration into the slope. Given the higher permeability of the sliding mass in the LG landslide compared to the YP landslide, the former was more susceptible to rainfall infiltration, leading to its sustained deformation. At the end of the flood season, the

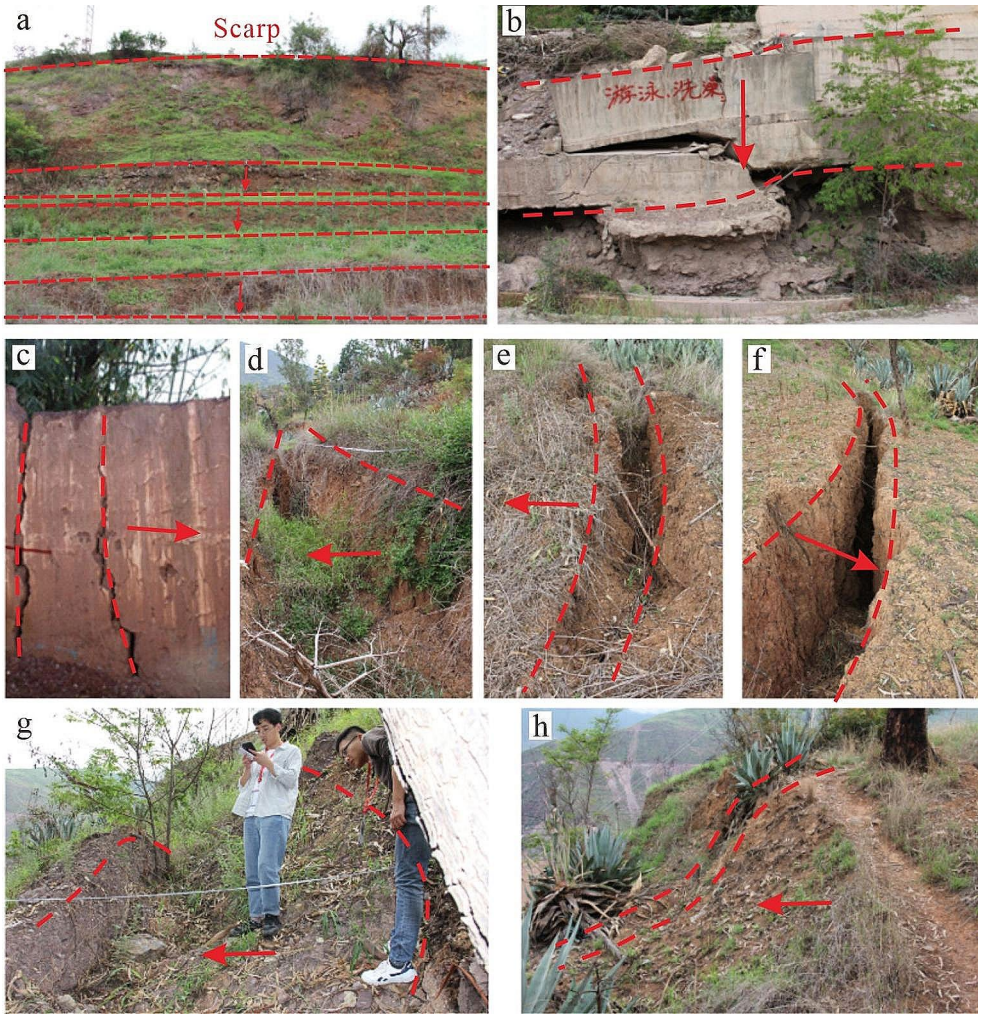

Fig. 8 Deformation of the YP landslide: **a** back scarp in I-1# zone, **b** road damages, **c** crack L5, **d** crack L7, **e** crack L8, **f** crack L9, **g** crack L11, and **h** crack L10

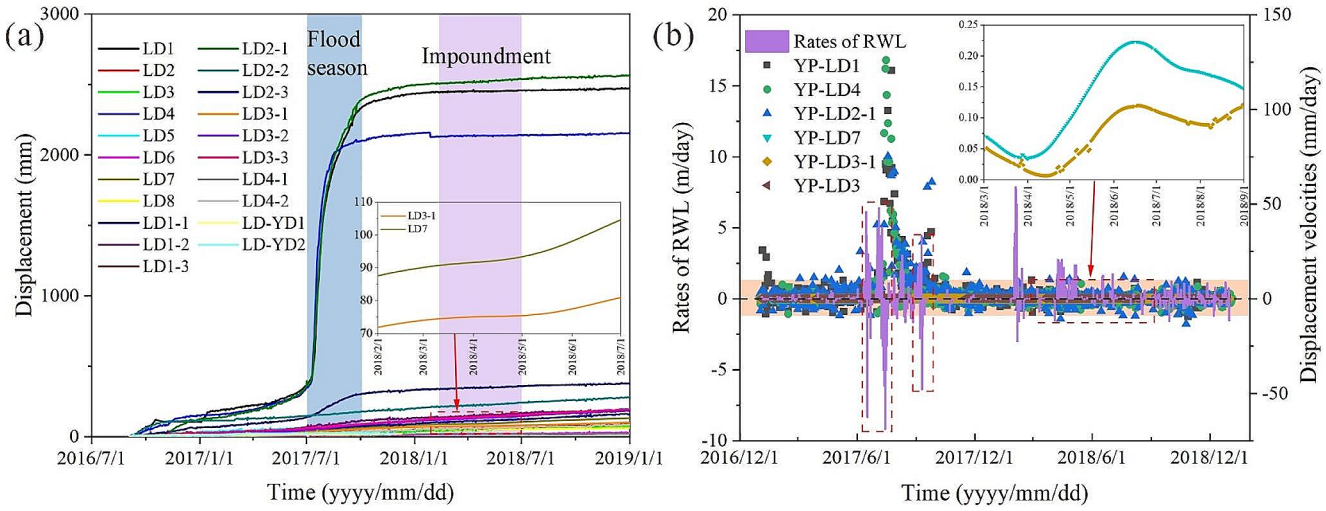

Fig. 9 Time-series of YP landslide: **a** surface displacement and **b** rates of RWL and GNSS

Table 1 Monthly displacement of representative GNSS monitoring sites from 2017 to 2018

Month	YP-LD4	YP-YD1	YP-LD6	YP-LD2-1	YP-LD2-2	YP-LD2-3	LG-LD1	LG-LD1-1	LG-LD1-2	LG-LD1-3	LG-LD1-4
201,701	6.06	/	-4.19	8.36	0.00	0.19	49.34	95.03	78.62	33.26	15.89
201,702	13.63	/	5.36	23.89	0.00	8.91	35.54	68.05	55.01	25.25	12.96
201,703	19.00	/	0.00	28.28	14.48	4.12	54.65	99.10	75.64	30.85	13.76
201,704	0.00	/	0.00	16.94	0.14	-4.04	60.27	103.95	71.79	37.04	5.82
201,705	0.00	/	3.39	40.46	0.71	-1.15	49.44	92.47	63.78	30.06	5.92
201,706	47.85	/	0.00	68.59	10.43	7.99	39.60	79.02	48.73	26.95	11.51
201,707	1403.85	/	-1.88	1258.07	8.23	3.36	135.87	114.27	78.04	37.78	5.82
201,708	277.71	/	2.27	470.80	9.62	8.18	213.5	213.93	132.08	54.86	6.44
201,709	38.97	/	4.71	235.37	11.32	8.69	226.69	276.99	170.39	56.88	20.81
201,710	28.62	/	0.16	56.67	9.33	7.42	95.56	190.21	125.87	45.74	12.43
201,711	10.80	3.67	0.26	28.57	3.24	1.02	40.13	95.02	72.47	26.72	4.82
201,712	8.38	0.74	-3.03	18.62	5.75	5.62	23.94	81.15	52.31	21.00	1.28
201,801	-23.77	2.58	0.78	12.32	15.93	11.89	15.50	21.76	31.63	14.90	19.05
201,802	5.81	0.96	2.63	3.43	5.57	3.56	9.89	42.25	17.86	8.33	2.41
201,803	4.02	-0.27	2.79	7.63	10.04	12.63	10.17	27.05	17.36	8.24	5.31
201,804	0.15	-1.22	1.64	3.40	8.68	3.38	8.18	22.54	14.97	6.21	4.63
201,805	1.57	-0.68	0.06	10.40	5.25	3.63	36.56	26.99	25.12	17.47	-1.95
201,806	7.19	-0.74	2.75	13.13	10.74	5.45	293.18	62.12	45.08	15.94	3.20
201,807	0.88	1.16	-0.23	8.68	7.17	6.29	255.85	119.60	76.98	20.90	9.12
201,808	1.73	-1.91	-1.36	1.27	5.75	6.30	664.86	207.02	137.79	29.30	2.88
201,809	-3.19	0.37	2.28	4.17	6.39	6.45	505.98	100.67	87.11	25.08	-2.02
201,810	1.19	1.45	-1.69	-5.73	-0.06	-0.83	308.05	28.61	19.49	18.53	5.52
201,811	4.07	1.09	-2.17	-1.60	4.26	7.08	463.58	34.16	25.98	24.77	1.11
201,812	3.56	4.28	2.86	3.93	4.98	0.19	715.89	9.78	4.20	25.52	1.43

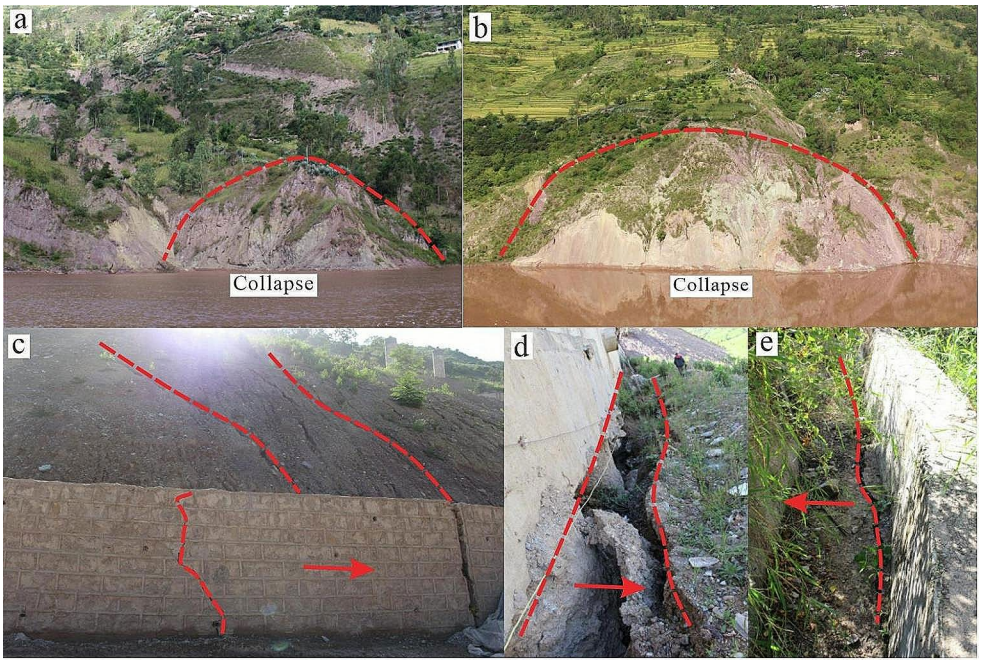

Fig. 10 Deformation of the LG landslide: **a** Collapse in I# zone, **b** Collapse in II-1# zone, **c** crack L4, **d** crack L5, and **e** crack L6

rate of landslide displacement decreased significantly and re-entered a low-velocity creep phase.

Landslides remained slowly deformed during the first rapid water storage phase in 2018 (Fig. 11b - third red box). Entering the second phase, characterized by slow filling, the displacement rate of each monitoring point began to increase, and the maximum displacement rate of LG-LD1 reached 39.35 mm/day, which was 40 times the low-speed creep rates (Fig. 11b - fourth red box). Subsequently, the displacement rate decreased, and the landslide re-entered the low-velocity creep stage. However, the displacement rate at monitoring point LG-LD1 continued to switch between

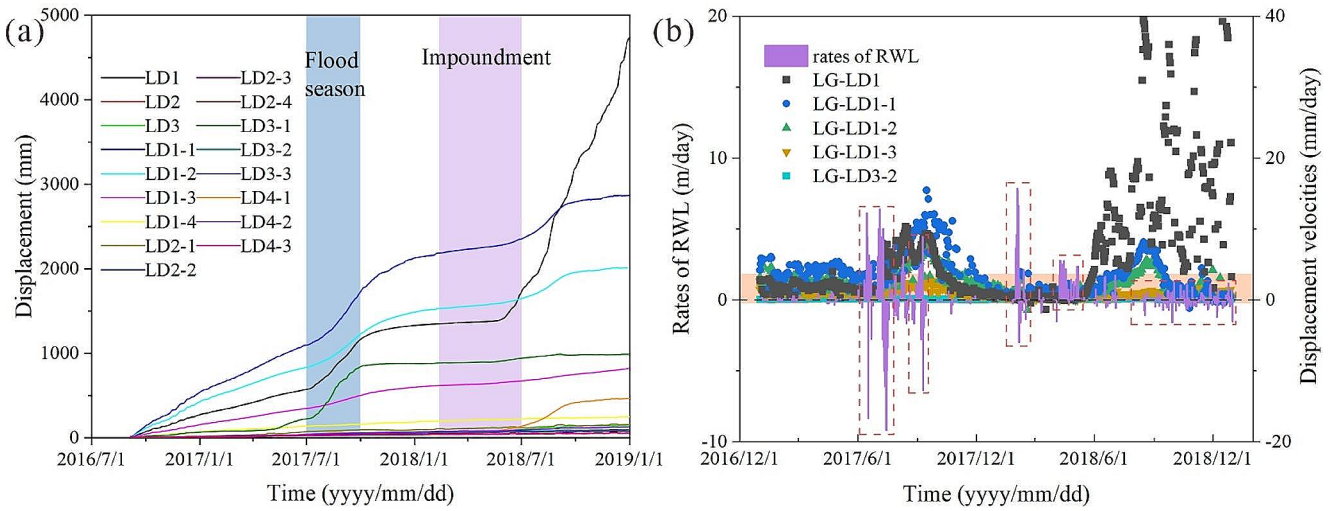

Fig. 11 Time-series of LG landslide: **a** surface displacement and **b** rates of RWL and GNSS

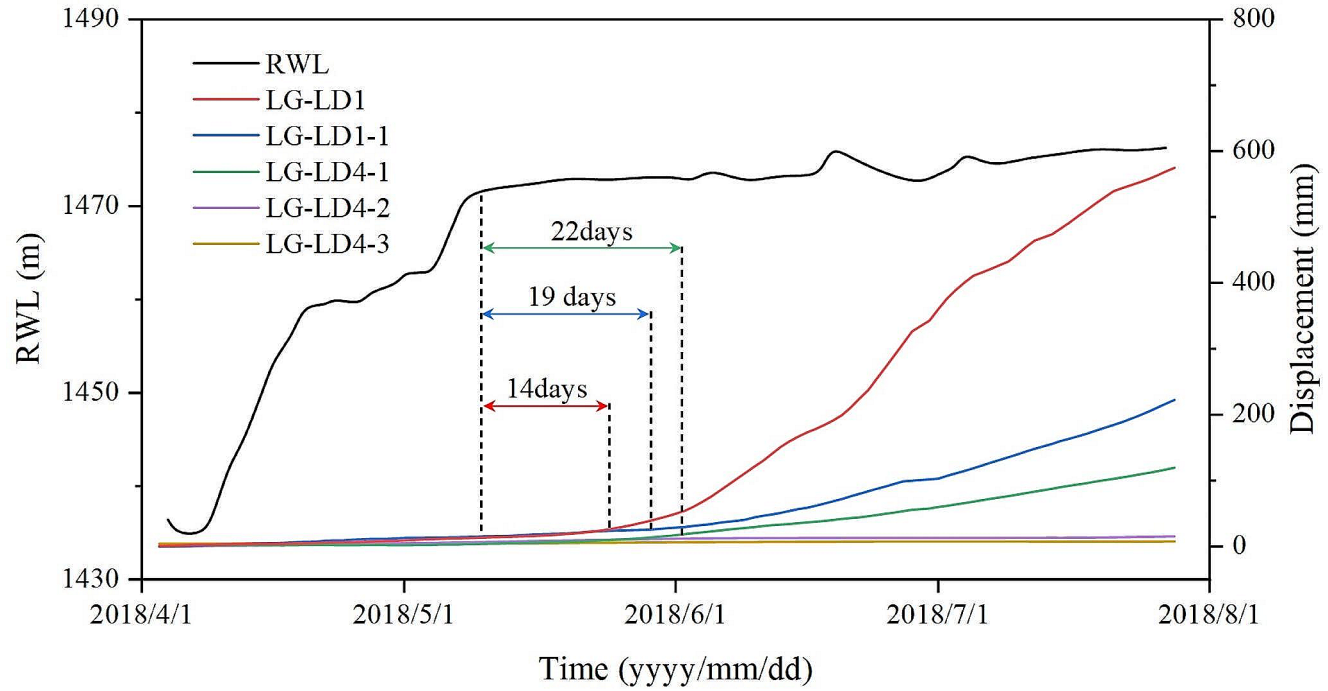

Fig. 12 Difference in response time after impoundment

high and low velocities, possibly due to the fact that this monitoring point is located at the foot of the landslide and in I# where deformation is intense, and the frequent fluctuations in RWL have resulted in a local collapse of the slope surface (Figs. 8b and 11b - fifth red box).

After the RWL reached 1472 m, the initial response of the LG landslide had a significant lag compared to the RWL rise (Fig. 12). The monitoring point data show that the time interval between the end moment of water storage and the beginning moment of accelerated deformation at monitoring points LG-LD1, LG-LD1-1, and LG-LD4-1 are 14, 19, and 22 days, respectively, while monitoring points at the back edge of the landslide, such as LG-LD4-2 and LG-LD4-3, show no turning point. It can be seen that the duration of response time is related to the location of the monitoring sites; the closer the points to Lancang River the shorter the response time, and the reservoir storage has less influence on the middle and rear part of the landslide. The LG landslide is, therefore, a typical retrogressive landslide, with deformation developing from front to back, similar to most reservoir landslides (Zhang et al. 2024).

Subsurface deformation

YP landslide

The displacement curves measured by the inclinometers and SAA of the YP landslide are shown in Fig. 13. The landslide displacement decreases with depth, and data from YP-SAA2-1 and YP-SAA3-1 located in the toe of the landslide exhibit obvious shear movement at 48 m and 29 m, respectively, which is essentially consistent with the location of the sliding zone revealed by the borehole. In general, the subsurface displacement of the landslide is larger the closer it is to the Lancang River, consistent with the surface displacement. There was no significant sliding surface formed at YP-IN2-1 in the rear of the landslide. These results suggesting that the landslide moved towards the toe of the slope (downwards), the movement is progressive from front to back.

YP-IN1-3 and YP-SAA3-1, located on the leading edge of the Yingpan landslide, underwent abrupt deformation in

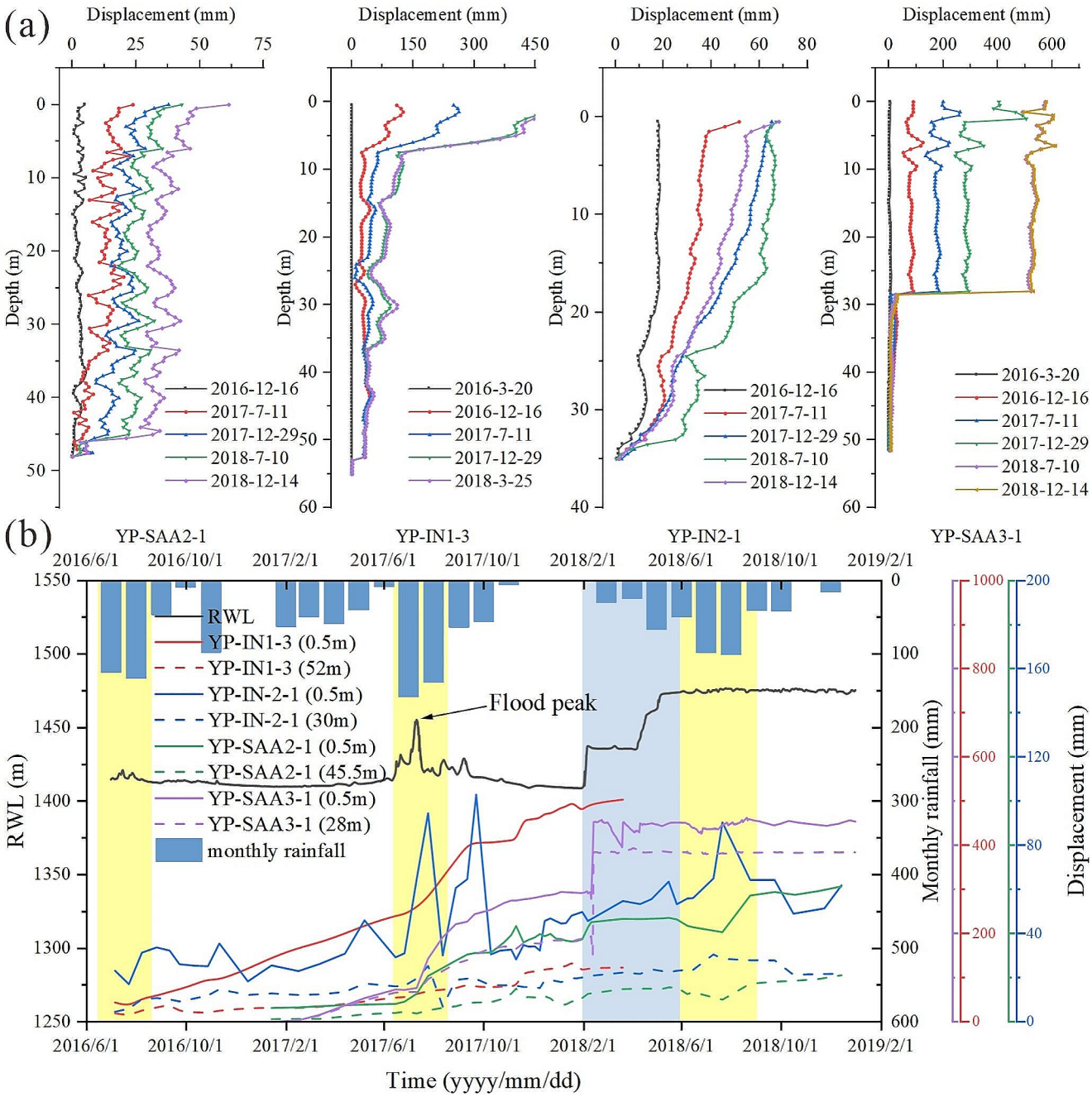

Fig. 13 Displacements measured by the inclinometers and SAA of YP landslide: **a** internal displacement; **b** time-series of RWL, rainfall, and displacement

July 2017, corresponding to the rapid fluctuations in RWL caused by floods. However, this accelerating phenomenon can only be observed in the shallow displacements (0.5 m) of the landslides; the deeper displacements of YP-IN1-3, YP-IN2-1, and YP-SAA2-1 do not show this character. In addition, the curve of YP-SAA3-1 shows a clear turning point in February 2018, suggesting that the reservoir storage has an effect on the downstream side of the Yingpan landslide, where stabilizing piles were not used. The stabilizing pile has a significant impact on the leading edge of the YP landslide, and the cumulative displacement of YP-IN1-3 for two years before pile implantation is about 450 mm (Fig. 13b). After the use of the stabilizing pile, the displacement curves in 2018 almost overlap, indicating that the deformation of the slope at this location is barely affected by impoundment. YP-IN2-1 lies in the middle of the landslide and keeps on creeping at a low rate throughout the observation period, with a maximum accumulated displacement of 68 mm, but displays an abrupt shift in July 2017, September 2017, and August 2018, which corresponds to constant precipitation.

LG landslide

As shown in Fig. 14a, the LG-IN2-1and LG-SAA1-1 at the toe of the sliding mass showed significant shear displacement at depths of 57 m and 43.5 m, while no apparent sliding surface was found at the LG-IN3-3 point on the rear edge, and the displacement was much less than that of the leading edge. This phenomenon is consistent with the results of the aforementioned field investigations and surface displacement monitoring, where LG landslide deformation developed from front to back. The displacement of a landslide diminishes with depth, with small deformation concentrated in a shear zone near bedrock, whereas the destabilized slip mass above the shear zone is influenced by greater strains and moves like a rigid body.

Figure 14b demonstrates the relationship between the deformation and the RWL and precipitation. There were three accelerated deformations of the LG landslide: the first was from July to August 2016, with two months of cumulative rainfall up to 268 mm; the second was in July 2017, corresponding to a continuous increase in rainfall and rapid fluctuations in RWL; and the third occurred during the slow reservoir storage phase and continued to accelerate after the onset of the rainy season. No data was collected for LG-SAA1-1 from July to October 2017. According to the available data, its displacement increased from 40.38 mm to 14.25 mm on 25 June to 183.50 mm and 77.98 mm on 23 November; hence it is presumed that the landslide underwent rapid deformation in flood season. On this basis, the missing displacement records are projected and supplemented to the full displacement curve using the black solid and dashed lines (Fig. 14b). A noteworthy point is that the deeper part of the landslide did not follow the rapid deformation of the shallow surface for the first two occasions but only followed the same trend after the water filling. In other words, the effects of rainfall and flood on the landslide were mainly concentrated on the slope surface, while impoundment caused increased deformation in the deeper parts.

Discussion

Triggering factors of the landslide deformation acceleration

There was accelerated deformation of the two ancient landslides due to the effects of flooding, impoundment, and rainfall; however, it remains uncertain which one is the governing factor. Consequently, the Pearson Correlation Coefficient was applied to quantitatively identify the triggering factor (Song et al. 2018). The correlation coefficients r and significance Sig. of landslide surface displacements with different hydrological factors are shown in Tables 2 and 3.

Table 2 shows the response of deformation to flooding and rainfall. The daily displacements and daily rainfall at four monitoring points at the leading edge of the YP landslide and the LG landslide from June to July 2017 were selected for the calculations. The water level changed rapidly before and after the flood event, so daily water levels were chosen to represent the contribution of the flood. For monitoring points YP-LD2-1, YP-LD4, LG-LD1, and LG-LD3-1, the r values between displacement and flood are negative, and their absolute values are all greater than 0.68, indicating a negative correlation between both. Landslide deformation increases when the reservoir level decreases. Hence, the water level decreased rapidly after the 2017 flood event, resulting in the landslide deformation. The absolute values of the coefficient r between displacement and rainfall are all less than 0.2, and those of the Sig. are greater than 0.05. There are no statistical correlations between displacement and rainfall. Thus, it can be concluded that flooding was the triggering factor for the first accelerated deformation of the two landslides.

Table 3 calculates the correlation of deformation to reservoir impoundment and rainfall, and the data used were monthly displacements at representative monitoring points, monthly reservoir level elevations, and monthly rainfall from January to October 2018. For the LG landslide, the r values between displacement and impoundment are both greater than 0.691, and the Sig. ones are less than 0.05, suggesting that there is a significant positive correlation between reservoir impoundment and accelerated deformation of the

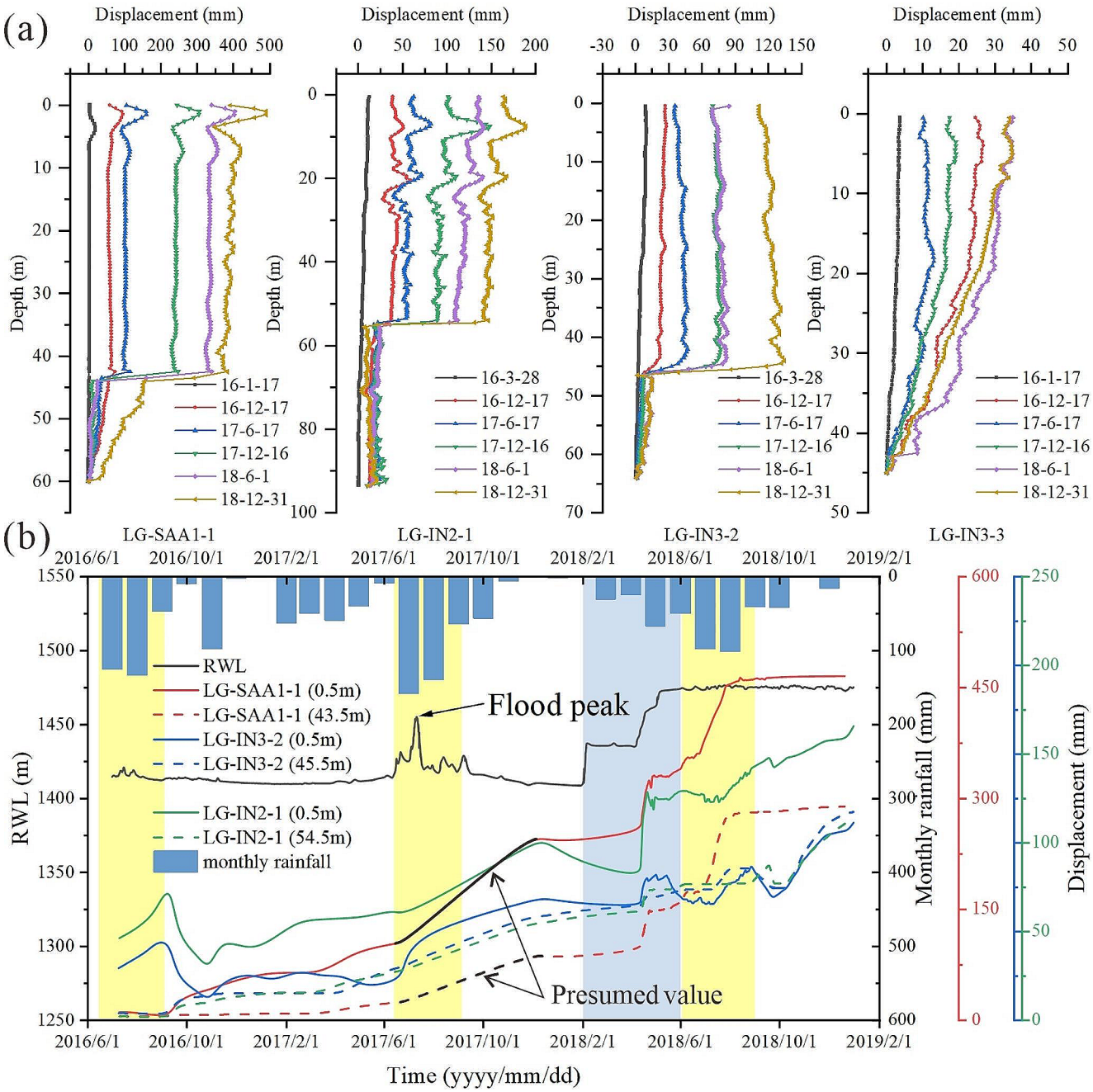

Fig. 14 Displacements measured by the inclinometers and SAA of LG landslide: **a** internal displacement; **b** time-series of RWL, rainfall, and displacement

Table 2 Correlations of displacement vs. flood and rainfall

Point number	Flood		Rainfall	
	r	Sig.	*r*	Sig.
YP-LD2-1	-0.779*	0.000	-0.200	0.274
YP-LD4	-0.739*	0.000	-0.205	0.260
LG-LD1	-0.684*	0.000	-0.244	0.178
LG-LD3-1	-0.709*	0.000	-0.251	0.166

Note r is the Pearson correlation coefficient and Sig. is the significance; *represents the values of Sig. less than 0.05, which means significant correlation

Table 3 Correlations of displacement vs. impoundment and rainfall

Point number	Impoundment		Rainfall	
	r	Sig.	*r*	Sig.
YP-LD2-1	0.176	0.650	0.482	0.189
YP-LD4	0.424	0.256	0.692*	0.039
LG-LD1	0.710*	0.021	0.696*	0.026
LG-LD4-1	0.691*	0.027	0.639*	0.047

Note r is the Pearson correlation coefficient and Sig. is the significance; *represents the values of Sig. less than 0.05, which means significant correlation

landslide. The *r* values between the displacement and rainfall are smaller than those between the former and impoundment, but for LG-LD1 and LG-LD4-1 they also reached 0.696 and 0.639, respectively. Therefore, impoundment and rainfall can be considered as controlling factors for the second accelerated deformation of the LG landslide, with the former playing a greater role than the latter. For the YP landslide, of the four correlation coefficients, only the one between LD4 and rainfall was greater than 0.6 and passed the significance test. This means that, statistically, impoundment has less of an effect on YP landslide movement.

Reactivation mechanisms

First acceleration deformation

Persistent rainfall or heavy storms are common in southwestern China from June to August, sometimes resulting in further flooding. Current research on the effects of the rainy season on landslides has primarily focused on different types of rainfall. Interestingly, this study found that flood event directly contributes to the reactivation of landslides. As shown in Fig. 15, the landslide did not occur at an accelerated deformation after the sustained rainfall and RWL increase in June and July 2017. Instead, the GNSS curve changed rapidly and abruptly following the transit of the 20-year flood in the afternoon of July 10. The damage process of flood on the reservoir bank slope is manifested as the soil and rock on the surface leaving the embankment under the action of water flow, which modifies the stress field at the front of the bank slope. Some scholars have reported the phenomenon of sliding and collapse of reservoir bank slope under the action of scouring, shearing, and erosion of flood (Richards and Reddy 2005; Larsen and Montgomery 2012).

The constant washing of the slope surface by the flood with its rapid flow, results in the erosion of slope materials and downstream transport of particles. This action culminates in the thinning of the leading edge of the landslide, thereby creating space for its movement (Thorne and Tovey 1981; Hooke 2008). Concurrently, the high energy of a large flood can create significant shear forces on the slopes, causing blocks to break as a result of collisions and the slopes to collapse (Snyder et al. 2003; Julian and Torres 2006). A portion of the floodwater can penetrate the interior of the bank slope, potentially prompting the loosening and dissolution of soil particles and resulting in the loss of fine particles and seepage deformation, further undermining the stability of the slope (Dang 2021). The site survey revealed that prior to flood transit, the leading edge of both landslides had generally collapsed, there were many visible cracks, and the slope material was severely broken (Fig. 16a and d). It is, therefore, very easy for the landslide surface material to be washed away and cause traction deformation during flood transit.

Besides, the flood causes a rapid shift in the RWL; in particular, a rapid drop in the RWL leads to a movement of the reservoir bank (Abam 1993; Wang et al. 2015). Over the course of the 2017 flood season, the RWL began to rise, reaching a cumulative height of 42 m in 30 days by 10 July. Broken ground provides favorable conditions for infiltration of reservoir water. The infiltration of reservoir water produced a deterioration effect on the geomaterials and reduced their shear strength, while the buoyancy force of the submerged part of the slope increased and the anti-sliding force decreased, which is not conducive to landslide stability. Nevertheless, the permeability coefficient of two landslides mass is between "medium" and "weak", so the rate of groundwater level rise lags behind that of the reservoir level. The seepage at the foot of the slope causes a continuous increase in dynamic water pressure (Tang et al. 2019b). Furthermore, the hydrostatic pressure generated by the high RWL outside the slope provides a supporting effect for the lateral deformation of the landslide (Paronuzzi et al. 2013). The combined action of the above two balances the

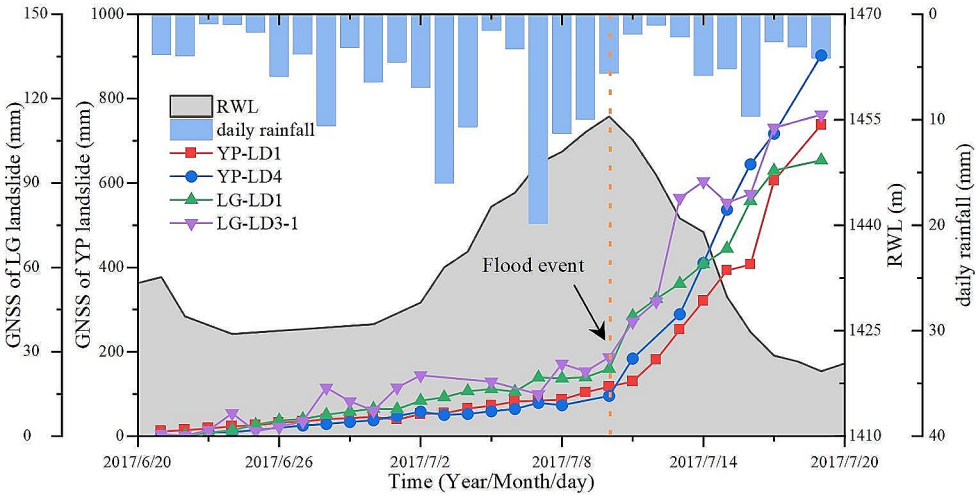

Fig. 15 Time series of RWL, daily rainfall, and GNSS data during the 2017 flood event

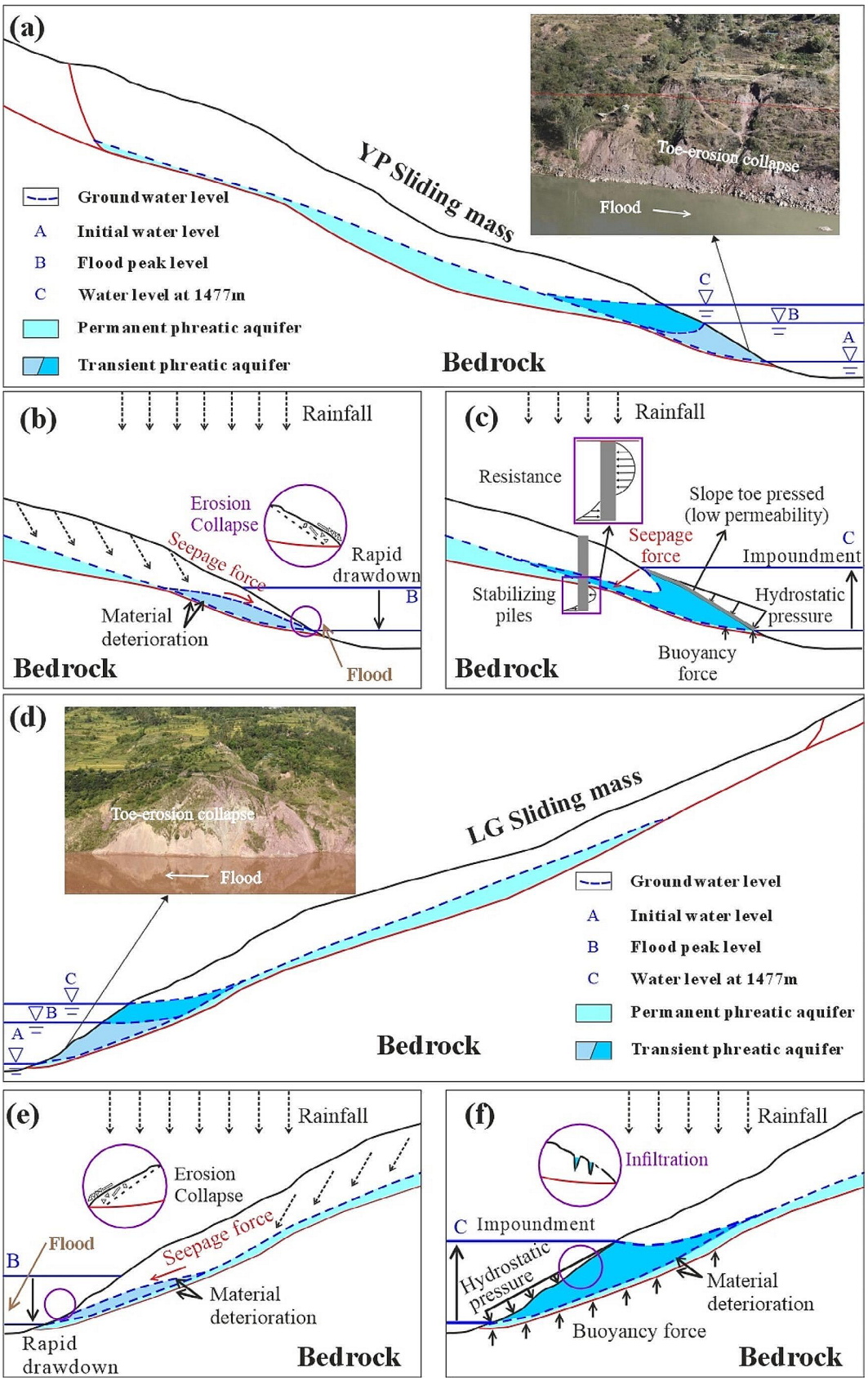

Fig. 16 Reactivation mechanisms of landslide subjected to flood, impoundment, and rainfall

negative effects of landslide deformation (Xia et al. 2013; Zou et al. 2021). After the flood passed on 10 July, the RWL dropped rapidly, dropping 35 m in 8 days, with the biggest daily drop being 8.9 m. The GNSS monitoring curve of the YP landslide rose steeply, with the highest displacement reaching about 700 mm within a few days, and the largest cumulative displacement in July being about 1403 mm. The LG landslide has also entered the accelerated deformation stage. This phenomenon can be explained by three possible reasons (Fig. 16b and e). Firstly, the sudden drop in RWL resulted in a rapid loss of buttressing effect at the toe of the slope (Paronuzzi et al. 2013; Wu et al. 2022). Second, the landslide soil was subjected to alternating wet and dry conditions, it is difficult to restore shear strength quickly in a short time. Third, the groundwater drawdown lagged behind the RWL since the permeability coefficient of the sliding mass is less than the rate of RWL fall. The rapid fall of the reservoir water created a higher hydraulic gradient, which created a greater seepage force, according to Darcy's Law, that pulled the landslide toward the valley (Song et al. 2018). The landslide reactivated and entered the first accelerated deformation phase. This type of landslide is often referred to as a seepage-driven landslide (Zhou et al. 2022). Since the permeability of the LG landslide is better than that of the YP, the head difference produced by the former is smaller than that of the latter, which in turn produces a smaller seepage force. The difference in displacement increments between the two landslides in July 2017 confirmed this, with the LG landslide being much smaller than the YP landslide (Figs. 9a and 11a; Table 1).

Floods often occur in the rainy season. It is worth noting that precipitation is not the primary driving factor for the two landslides. As an example, several long-term or heavy rainfall events occurred in June and early July 2017, but no large displacements were observed (Fig. 15). A significant acceleration did not occur until 10 July, when floods moved in and the RWL began to decline.

In conclusion, the mechanism of the first accelerated deformation of the two landslides is similar. The direct triggering factors were flood-induced scouring, shearing, erosion, and rapid drawdown in water level.

Second acceleration deformation

The experience gained from the construction of many hydropower stations shows that reservoir impoundment leads to the reactivation of ancient landslides (Chen et al. 2018; Tang et al. 2019a). As mentioned before, the impoundment process of Dahuaqiao Reservoir is divided into two phases: rapid impoundment in a short time and continuous impoundment (Fig. 2b). In the first stage, the RWL rose by 25 m in 5 days, which was too fast and made it difficult for the reservoir water to infiltrate into the slope in time to raise the groundwater level. By this time, the hydrostatic pressure provided a dominant supporting effect, and the LG landslide continued to move slowly (Figs. 11 and 14b). Another possible reason is that the landslide developed adaptive capacity after the 2017 RWL change, so when the initial filling height did not exceed the 2017 peak, the landslide deformation did not accelerate (He et al. 2020). In the second stage, the reservoir water can continue to supply groundwater when the reservoir level rises due to the small difference between the filling rate and the permeability coefficient of LG landslide sliding mass, resulting in an elevation of the groundwater level (Tang et al. 2019b; Yi et al. 2022). At this point, more parts of the slope were submerged. The pore water pressure of the landslide increased, the effective stress reduced, and the landslide's anti-slip force was weakened by the floating weight-reducing effect due to the ongoing increase in buoyancy (Fig. 16f). Additionally, the invasion of reservoir water led to the softening, lubrication, and argillation of the sliding mass and zone, reducing their mechanical strength. Thus, the dynamic equilibrium between the negative effect and the supporting effect was broken, which eventually led to the second rapid deformation of the LG landslide. These features are usually considered to be characteristic of buoyancy-driven landslides (Xia et al. 2019; Zhou et al. 2022; Yi et al. 2022). After impoundment was completed, the RWL fluctuated between 1472 and 1477 m, and the landslide deformation reentered the creep phase with low velocity. However, the deformation rate of the monitoring point LG-LD1 didn't reduce, and the displacement continued to grow at a fast rate. Given that the LG-LD1 monitoring station is located on a scarp close to the leading edge of the landslide (Fig. 5b), the frequent fluctuations of the RWL may have caused significant denudation on the scarp, resulting in persistent deformation.

The YP landslide maintained a uniform deformation at a low rate during the entire impoundment, which is owing to the reinforcing methods of stabilizing piles and slope toe pressed utilized prior to water storage (Fig. 16e). The former greatly improved landslide stability by transferring the sliding force of the sliding mass into the stable bedrock, whereas the latter limited spalling of the slope surface due to frequent fluctuations in RWL and mitigated the infiltration of reservoir water; the seepage force pointing into the slope also helped to restrict landslide deformation (Fig. 16d) (Li et al. 2009; Tang et al. 2023). The shear strength of the landslide materials decreased after three months of immersion, and the movement rate increased slightly on the downstream side in the I-1# zone during the second stage of water storage due to the lack of stabilizing piles (Fig. 7a). However, it should be noted that the acceleration was still quite tiny with a maximum displacement rate of around 0.29 mm/

day. However, in the long term, impoundment will reduce slope stability due to the accumulation of damage within the material being moved (Luo et al. 2019).

Rainfall is another factor that promotes the deformation of the reservoir landslides. Rainfall infiltration not only increases the water content of the sliding mass and sliding zone and weakens the shear strength but also enhances the pore water pressure and reduces the effective stress (Wang and Sassa 2003; Collins and Znidarcic 2004; Wang et al. 2022) (Fig. 16b and e). Rainfall has a greater impact on the LG landslide than the YP landslide, due to differences in permeability. In addition, the leading edge of the LG landslide has not been treated in any way and the broken surface is very favorable for rain infiltration (Fig. 16f). Hence, the movement of the LG landslide accelerated into the rainy season. The calculated results of the correlations in Sect. 5.1 support this conclusion.

The LG landslide showed a second accelerated deformation after impoundment, while the YP landslide did not. The discrepancy in the observed results can be attributed to two factors. On the one hand, the permeability of the LG landslide is better than that of the YP landslide, which is more favorable to the infiltration of reservoir water and rainfall. On the other hand, the treatment works changed the evolutionary stage of the YP landslide, and the landslide re-entered the creep stage (Hu et al. 2019).

Conclusions

In this paper, the deformation features and reactivation mechanisms of the Yingpan and Lagu landslides subjected to flood and impoundment of the Dahuaqiao Reservoir are elucidated through a combined analysis of geological investigations and in-situ monitoring. The following are the main conclusions:

(1) The two ancient landslides were in a low-velocity creep state most of the time and were reactivated as a result of changes in the hydraulic conditions. In 2017, the 20-year flood directly led to accelerated deformation of the two landslides, with the YP landslide showing an abrupt change in cumulative surface displacement and its speed and the LG landslide showing a continuous increase in displacement rate until the end of the rainy season. In 2018, the shallow and deep displacements of the LG landslide showed an obvious response to reservoir impoundment, and the lower the altitude, the faster the response. The YP landslide and the LG landslide are both retrogressive landslides because the influence of the flood and impoundment is mainly concentrated on the leading edge of the two landslides. The effects of the flood focused on the shallow surface, while the impoundment caused overall deformation.

(2) Although the YP and LG landslides are only 12 km apart and share similar geological conditions, their reaction to various hydrological factors is distinct because of the difference in permeability and the presence or absence of reinforcement. Correlation analyses reveal that the decrease in water level due to flooding is negatively correlated with the initial accelerated deformation of both landslides, with a small impact from rainfall. Reservoir impoundment and rainfall are strongly positively correlated with the secondary accelerated deformation of the LG landslide while showing no statistical correlation with the YP landslide.

(3) In the first acceleration movement, the deformation mechanisms are similar for both landslides: Floods caused rapid rise and fall of water level. When the water level rapidly draws down, the immediate loss of buttressing effect, the continuous increase in seepage force, and the deterioration of the geotechnical material after soaking, coupled with the action of scouring, shearing, and erosion of flood, together lead to accelerated deformation of landslides. In the second acceleration movement, the deformation mechanisms are different: The LG landslide exhibits a higher coefficient of permeability compared to the YP landslide. After impoundment, the leading edge of the LG landslide was submerged. The reservoir water gradually increased the buoyancy force on the landslide mass, leading to a reduction in normal stress on the sliding surface and a decrease in resisting force. Concurrently, infiltration of rainwater contributed to a reduction in effective stress. Collectively, these effects precipitated the rapid movement of the landslide. The YP landslide was reinforced with slope toe pressed and stabilizing piles prior to impoundment. The former slowed down the infiltration of the reservoir water and rainfall, while the latter reduced the landslide sliding force by transferring the landslide thrust to the stabilized bedrock. Together, they ensure the stability of the YP landslide during and after the impoundment process.

At present, the deformation rate of the two landslides has decreased following rapid movement, reverting to a creep phase characterized by low velocity. However, long-term RWL fluctuations may cause damage to the forward edge of the landslides; thus, continued monitoring of both landslides is essential to understand their deformation mechanisms further.

Acknowledgements This work was supported by the Major International (Regional) Joint Research Project of the NSFC (No. 42020104006) and the National Major Scientific Instruments and Equipment Development Projects of China (No. 41827808). The authors appreciate Huaneng Lancang River Hydropower Inc. for providing sufficient monitoring data. The authors also wish to thank the editors and anonymous reviewers for their valuable suggestions to improve the manuscript.

Data availability Data used for this article are available from the corresponding author upon reasonable request.

Declarations

Conflict of interest The authors declare that they have no known competing financial interests or personal relationships that could have appeared to influence the work reported in this paper.

References

Abam TKS (1993) Factors affecting distribution of instability of river banks in the Niger delta. Eng Geol 35:123–133. https://doi.org/10.1016/0013-7952(93)90074-M

Chen ML, Lv PF, Zhang SL et al (2018) Time evolution and spatial accumulation of progressive failure for Xinhua slope in the Dagangshan reservoir, Southwest China. Landslides 15:565–580. https://doi.org/10.1007/s10346-018-0946-8

Collins BD, Znidarcic D (2004) Stability analyses of rainfall induced landslides. J Geotech Geoenviron Eng 130:362–372. https://doi.org/10.1061/(ASCE)1090-0241(2004)130:4(362)

Cruden DM, Varnes DJ (1996) Landslide types and processes. In: Turner AK, Schuster RL (eds) Landslides investigation and mitigation. Transportation research board, US National Research Council. Special Report 247, Washington, DC, Chap. 3, pp. 36–75

Dang YD (2021) Study on deformation of bank collapse due to flood erosion based on particle flow code -- a case study of Ganquan County, Beiluo River. Dissertation, Chang'an University. (in Chinese) https://doi.org/10.26976/d.cnki.gchau. 2021.000206

He CC, Hu XL, Xu C et al (2020) Model test of the influence of cyclic water level fluctuations on a landslide. J Mt Sci 17:191–202. https://doi.org/10.1007/s11629-019-5713-9

Hooke JM (2008) Temporal variations in fluvial processes on an active meandering river over a 20-year period. Geomorphology 100:3–13. https://doi.org/10.1016/j.geomorph.2007.04.034

Hu XL, Zhou C, Xu C et al (2019) Model tests of the response of landslide-stabilizing piles to piles with different stiffness. Landslides 16:2187–2200. https://doi.org/10.1007/s10346-019-01233-4

Huang QX, Wang JL, Xue X (2016) Interpreting the influence of rainfall and reservoir infilling on a landslide. Landslides 13:1139–1149. https://doi.org/10.1007/s10346-015-0644-8

Huang D, Luo SL, Zhong Z et al (2020a) Analysis and modeling of the combined effects of hydrological factors on a reservoir bank slope in the Three Gorges Reservoir area, China. Eng Geol 279:105858. https://doi.org/10.1016/j.enggeo.2020.105858

Huang XH, Guo F, Deng ML et al (2020b) Understanding the deformation mechanism and threshold reservoir level of the floating weight-reducing landslide in the Three Gorges Reservoir Area, China. Landslides 17:2879–2894. https://doi.org/10.1007/s10346-020-01435-1

Hungr O, Leroueil S, Picarelli L (2014) The Varnes classification of landslide types, an update. Landslides 11:167–194. https://doi.org/10.1007/s10346-013-0436-y

Iqbal J, Dai F, Hong M et al (2018) Failure mechanism and stability analysis of an active landslide in the Xiangjiaba reservoir area, southwest China. J Earth Sci 29:646–661. https://doi.org/10.1007/s12583-017-0753-5

Jiang ZH, Wang HL, Xie W (2021) Deformation mechanism of deposit landslide induced by fluctuations of reservoir water level based on physical model tests. Environ Earth Sci 80:1–13. https://doi.org/10.1007/s12665-021-09673-9

Julian JP, Torres R (2006) Hydraulic erosion of cohesive riverbanks. Geomorphology 76:193–206. https://doi.org/10.1016/j.geomorph.2005.11.003

Kilburn CRJ, Petley DN (2003) Forecasting giant, catastrophic slope collapse: lessons from Vajont, Northern Italy. Geomorphology 54:21–32. https://doi.org/10.1016/S0169-555X(03)00052-7

Larsen IJ, Montgomery DR (2012) Landslide erosion coupled to tectonics and river incision. Nat Geosci 5:468–473. https://doi.org/10.1038/ngeo1479

Li TL, Zhang CL, Xu P et al (2009) Stability assessment and stabilizing approaches for the Majiagou landslide, undergoing the effects of water level fluctuation in the Three Gorges Reservoir area. In: Wang F, Li T (eds) Landslide disaster mitigation in Three Gorges Reservoir, China. Environmental Science and Engineering. Springer, Berlin, Heidelberg. https://doi.org/10.1007/978-3-642-00132-1_14

Lin YS, Wang JL, Wang J et al (2017) Report on the prevention and control design of Cangjiangqiao-Yingpan landslide in Dahuaqiao Hydropower Station on the Lancang River in Yunnan. Beijing. (in Chinese)

Luo SL, Jin XG, Huang D (2019) Long-term coupled effects of hydrological factors on kinematic responses of a reactivated landslide in the Three Gorges Reservoir. Eng Geol 261:105271. https://doi.org/10.1016/j.enggeo.2019.105271

Paronuzzi P, Rigo E, Bolla A (2013) Influence of filling-drawdown cycles of the Vajont reservoir on Mt. Toc slope stability. Geomorphology 191:75–93. https://doi.org/10.1016/j.geomorph.2013.03.004

Rahardjo H, Ong TH, Rezaur RB et al (2007) Factors controlling instability of homogeneous soil slopes under rainfall. J Geotech Geoenviron Eng 133:1532–1543. https://doi.org/10.1061/(ASCE)1090-0241(2007)133:12(1532)

Ran Q, Hong Y, Li W et al (2018) A modelling study of rainfall-induced shallow landslide mechanisms under different rainfall characteristics. J Hydrol 563:790–801. https://doi.org/10.1016/j.jhydrol.2018.06.040

Richards KS, Reddy KR (2005) Slope failure of embankment dam under extreme flooding conditions: comparison of limit equilibrium and continuum models. American Society of Civil Engineers, Austin, Texas, United States, pp 1–12. https://doi.org/10.1061/40787(166)30

Shi XG, Hu X, Sitar N et al (2021) Hydrological control shift from river level to rainfall in the reactivated Guobu slope besides the Laxiwa hydropower station in China. Remote Sens Environ 265:112664. https://doi.org/10.1016/j.rse.2021.112664

Snyder NP, Whipple KX, Tucker GE et al (2003) Importance of a stochastic distribution of floods and erosion thresholds in the bedrock river incision problem. J Geophys Res-Sol Ea 108(B2). https://doi.org/10.1029/2001JB001655

Song K, Wang FW, Yi QL et al (2018) Landslide deformation behavior influenced by water level fluctuations of the Three Gorges Reservoir (China). Eng Geol 247:58–68. https://doi.org/10.1016/j.enggeo.2018.10.020

Sun Q (2015) Rock alteration in a hydraulic engineering project in Southwest China. Arab J Geosci 8:23–27. https://doi.org/10.1007/s12517-013-1194-9

Tang HM, Wasowski J, Juang CH (2019a) Geohazards in the Three Gorges Reservoir Area, China - lessons learned from decades of research. Eng Geol 261:105267. https://doi.org/10.1016/j.enggeo.2019.105267

Tang MG, Xu Q, Yang H et al (2019b) Activity law and hydraulics mechanism of landslides with different sliding surface and permeability in the Three Gorges Reservoir Area, China. Eng Geol 260:105212. https://doi.org/10.1016/j.enggeo.2019.105212

Tang HM, Wang LQ, Li CD et al (2023) Key techniques of Prevention and Control for Reservoir landslides based on evolutionary process. In: Alcántara-Ayala I, Arbanas Ž, Huntley D et al (eds) Progress in Landslide Research and Technology, volume 1 issue

2, 2022. Springer International Publishing, Cham, pp 11–28. https://doi.org/10.1007/978-3-031-18471-0_2

Thorne CR, Tovey NK (1981) Stability of composite river banks. Earth Surf Proc Land 6:469–484. https://doi.org/10.1002/esp.3290060507

Wang G, Sassa K (2003) Pore-pressure generation and movement of rainfall-induced landslides: effects of grain size and fine-particle content. Eng Geol 69:109–125. https://doi.org/10.1016/S0013-7952(02)00268-5

Wang FW, Zhang YM, Huo ZT et al (2004) The July 14, 2003 Qianjiangping landslide, Three Gorges Reservoir, China. Landslides 1:157–162. https://doi.org/10.1007/s10346-004-0020-6

Wang TG, Kuang SF, C Y (2015) Impacts of water level fluctuations on bank stability during flood period. Shuili Xuebao 46(12):1398–1405 (in Chinese). https://doi.org/10.13243/j.cnki.slxb.20150490

Wang L, Chen Y, Wang S et al (2022) Response of landslide deformation to rainfall based on multi-index monitoring: a case of the Tanjiawan landslide in the Three Gorges Reservoir. Bull Eng Geol Environ 81:231. https://doi.org/10.1007/s10064-022-02732-w

Wu SS, Hu XL, Zheng WB et al (2021) Threshold definition for monitoring Gapa landslide under large variations in reservoir level using GNSS. Remote Sens 13(24):4977. https://doi.org/10.3390/rs13244977

Wu SS, Hu XL, Zheng WB et al (2022) Displacement behaviour and potential impulse waves of the Gapa landslide subjected to the Jinping Reservoir fluctuations in Southwest China. Geomorphology 397:108013. https://doi.org/10.1016/j.geomorph.2021.108013

Xia M, Ren GM, Ma XL (2013) Deformation and mechanism of landslide influenced by the effects of reservoir water and rainfall, three gorges, China. Nat Hazards 68:467–482. https://doi.org/10.1007/s11069-013-0634-x

Xia M, Ren GM, Li TB et al (2019) Complex rock slope deformation at Laxiwa Hydropower Station, China: background, characterization, and mechanism. Bull Eng Geol Environ 78:3323–3336. https://doi.org/10.1007/s10064-018-1371-x

Yang H, Song K, Chen L et al (2023) Hysteresis effect and seasonal step-like creep deformation of the Jiuxianping landslide in the Three Gorges Reservoir region. Eng Geol 317:107089. https://doi.org/10.1016/j.enggeo.2023.107089

Yao W, Li C, Zuo Q et al (2019) Spatiotemporal deformation characteristics and triggering factors of Baijiabao landslide in Three Gorges Reservoir region, China. Geomorphology 343:34–47. https://doi.org/10.1016/j.geomorph.2019.06.024

Yi X, Feng W, Wu M et al (2022) The initial impoundment of the Baihetan reservoir region (China) exacerbated the deformation of the Wangjiashan landslide: characteristics and mechanism. Landslides 19:1897–1912. https://doi.org/10.1007/s10346-022-01898-4

Yin YP, Wang HD, Gao YL et al (2010) Real-time monitoring and early warning of landslides at relocated Wushan Town, the Three Gorges Reservoir, China. Landslides 7:339–349. https://doi.org/10.1007/s10346-010-0220-1

Yin YP, Huang BL, Wang WP et al (2016) Reservoir-induced landslides and risk control in three gorges Project on Yangtze River, China. J Rock Mech Geotech 8:577–595. https://doi.org/10.1016/j.jrmge.2016.08.001

Zhang L, Zhu HH, Han HM et al (2024) Fiber optic monitoring of an anti-slide pile in a retrogressive landslide. J Rock Mech Geotech Eng 16:333–343. https://doi.org/10.1016/j.jrmge.2023.02.011

Zhao DP, Wang SM, Tan ZY et al (2013) Stability studies of buoyancy weight loss landslides under reservoir water level fluctuation. Rock Soil Mech 34(4):1017–1024 (in Chinese). https://doi.org/10.16285/j.rsm.2013.04.020

Zhou C, Cao Y, Yin KL et al (2022) Characteristic comparison of seepage-driven and buoyancy-driven landslides in Three Gorges Reservoir area, China. Eng Geol 301:106590. https://doi.org/10.1016/j.enggeo.2022.106590

Zou ZX, Tang HM, Criss RE et al (2021) A model for interpreting the deformation mechanism of reservoir landslides in the Three Gorges Reservoir area, China. Nat Hazards Earth Syst Sci 21:517–532. https://doi.org/10.5194/nhess-21-517-2021